Research Article

ADVANCED PHOTONICS

Ultrawideband chromatic aberration-free meta-mirrors

Tong Cai,[a,b,c,†] **Shiwei Tang,**[d,†] **Bin Zheng,**[a,c,*] **Guangming Wang,**[b] **Wenye Ji,**[b] **Chao Qian,**[a,c] **Zuojia Wang,**[a] **Erping Li,**[a,c] **and Hongsheng Chen**[a,c,*]

[a]Zhejiang University, College of Information Science and Electronic Engineering, Interdisciplinary Center for Quantum Information, State Key Laboratory of Modern Optical Instrumentation, Hangzhou, China
[b]Air Force Engineering University, Air and Missile Defend College, Xi'an, China
[c]Zhejiang University, ZJU-Hangzhou Global Science and Technology Innovation Center, Key Laboratory of Advanced Micro/Nano Electronic Devices and Smart Systems of Zhejiang, Hangzhou, China
[d]Ningbo University, Department of Physics, Faculty of Science, Ningbo, China

Abstract. Chromatic aberration-free meta-devices (e.g., achromatic meta-devices and abnormal chromatic meta-devices) play an essential role in modern science and technology. However, current efforts suffer the issues of low efficiency, narrow operating band, and limited wavefront manipulation capability. We propose a general strategy to design chromatic aberration-free meta-devices with high-efficiency and ultrabroadband properties, which is realized by satisfying the key criteria of desirable phase dispersion and high reflection amplitudes at the target frequency interval. The phase dispersion is tuned successfully based on a multi-resonant Lorentz model, and high reflection is guaranteed by the presence of the metallic ground. As proof of the concept, two microwave meta-devices are designed, fabricated, and experimentally characterized. An achromatic meta-mirror is proposed within 8 to 12 GHz, and another abnormal chromatic meta-mirror can tune the reflection angle as a linear function. Both meta-mirrors exhibit very high efficiencies (85% to 94% in the frequency band). Our findings open a door to realize chromatic aberration-free meta-devices with high efficiency and wideband properties and stimulate the realizations of chromatic aberration-free meta-devices with other functionalities or working at higher frequency.

Keywords: chromatic aberration-free meta-devices; ultrabroadband metasurface; phase and dispersion control; multiresonant Lorentz model.

1 Introduction

The manipulation of electromagnetic (EM) waves with high-efficiency and wideband is of great importance to increase the accuracy and efficiency of integrated optics components, especially for chromatic aberration-free meta-devices (e.g., achromatic meta-devices and abnormal chromatic meta-devices). With the advent of three-dimensional (3D) metamaterials, artificial materials consisting of subwavelength meta-atoms with tailored permeability and permittivity,[1,2] many EM wavefront control devices have been facilitated, such as polarization beam splitters,[3,4] perfect lenses,[5,6] and EM cloaks.[7,8] However, these devices are seriously limited by their bulky size, complex fabrication, narrow operation band, and low efficiencies due to the inherent resonant property and material dispersion. Recently, metasurfaces, as a planar version of 3D metamaterials, provide a powerful capability to manipulate the amplitude, phases, and polarizations of EM waves, leading to a lot of fascinating phenomena and effects, such as anomalous refraction and reflection,[9–12] planar meta-holograms,[13–16] achromatic meta-lenses,[17–26] surface plasmon polaritons meta-couplers,[27–30] multifunctional metasurfaces,[31–34] meta-cloaks,[35–39] and many others.[40–53] These metasurfaces, working at frequencies ranging from microwave

---

*Address all correspondence to Bin Zheng, zhengbin@zju.edu.cn; Hongsheng Chen, hansomchen@zju.edu.cn

†These authors contributed equally to this work.

to visible, have found a wide scope of applications in EM integration, optical imaging, target detection, as well as communication systems.[9–54]

Despite these achievements in metasurfaces realized so far, it is a great challenge to design chromatic aberration-free meta-devices with both high efficiencies and ultrabroad bandwidth. For one thing, most of the reported metasurfaces suffer from limited chromatic aberration ability and narrow bandwidth.[9–16,27–43,54] These metasurfaces are predesigned at a target frequency of f_0 with a certain phase gradient, and, as such, a pure single-mode EM functionality with high-efficiency can be observed at f_0 based on the generalized Snell's law.[9–12] However, the device performances and working efficiencies degrade significantly as the frequency is away from f_0 due to the intrinsically undesired dispersions of resonant meta-atoms. For another, the reported achromatic meta-devices are limited by low efficiencies and/or narrow bandwidth. For instance, some achromatic meta-lenses are engineered at only three separate frequencies,[17,18] and the dispersion cannot be tuned within a wide band. Some achromatic meta-devices, based on Pancharatnam–Berry (PB) metasurfaces, can work in a broad bandwidth,[25,26] while the efficiencies are very low due to the low reflection or transmission property of these metasurfaces. Therefore, to realize a chromatic aberration-free meta-device with high efficiency and ultrawideband properties, it is necessary to manipulate both the phase dispersion and reflection or transmission property at will.

In this paper, we propose a multiresonant Lorentz model to control both the phase dispersion and reflection amplitude, guided by the transfer-matrix-method (TMM).[44–46] Realistic three-resonant meta-atoms are designed and optimized to achieve desirable phase dispersion and high reflection distributions, yielding the realizations of chromatic aberration-free meta-devices with high-efficiency and wideband properties. As proof of the concept, five frequency-dependent meta-mirrors with different chromatisms are designed, which show the wideband chromatic property (same phase gradient within the working band, see details in Sec. H of the Supplemental Materials), achromatic property (same deflection angle within the working band, see the design of the THz and optical achromatic meta-mirrors in Sec. G of the Supplemental Materials), and abnormal chromatic property (deflection angle changes as a linear function within the working band), respectively. More importantly, all of these devices can cover a broadband (microwave meta-mirror within 8 to 12 GHz, THz case in 0.5 to 0.8 THz, optical case within 1150 to 1875 nm), and realize very high working efficiencies (microwave meta-mirror in the range of 85% to 94%, THz case in the range of 75% to 84%, and optical case in the range of 85% to 91%). Our findings provide a solid step in solving the major problem of integrating the efficiency and bandwidth in meta-devices.

2 Materials and Methods

In our previous works,[31,32] we have proposed the high-performance criteria for reflective and transmissive metasurfaces working at a target frequency of f_0 by satisfying high amplitudes and required phase distributions at certain positions. We now describe our strategy to design chromatic aberration-free meta-devices with high-efficiency and ultrawideband properties. As we know, the EM functionality of the meta-device can be determined by the total phase $\varphi_{tot}(r,\lambda) = \varphi_m(r,\lambda) + \varphi_p(r,\lambda)$,[17] with $\varphi_m(r,\lambda)$ being the phase imparted by the

metasurface, $\varphi_p(r,\lambda)$ being the phase accumulated by propagation length in free space, and λ being the wavelength at frequency of f.[17] Here, $\varphi_p(r,\lambda) = \frac{2\pi}{\lambda} l(r)$, with $l(r)$ being the distance between the interference at r and the desired wavefront. Therefore, to ensure high efficiency and wideband properties of chromatic aberration-free meta-devices, we need not only to control the phase dispersion $\varphi_m(r,\lambda)$ as a function of frequency within an ultrabroad band but also to control the corresponding amplitudes (reflection or transmission) of the metasurface close to unit. Here, we adopt a reflective system working at the X band (8 to 12 GHz) with global mirror symmetries to control the dispersion efficiently.[31,32,44–46] The reflective amplitude keeps close to unit because of the presence of a metallic ground layer, which can naturally reflect all incoming waves back. In this way, the key step is to control the distributions of $\varphi_m(r,\lambda_i)$ at local positions.

Take a meta-mirror as an example, the dispersion φ_m should compensate at each frequency as

$$\varphi_m(r,\lambda_i) = -\frac{2\pi}{\lambda_i} \sin[\theta_i(f_i)]x + \varphi_0, \tag{1}$$

where $\theta_i(f_i)$ is the predesigned deflection angle, λ_i is the wavelength at f_i, and φ_0 is an initial phase. For a conventional chromatic meta-mirror,[9–16] the phase difference between adjacent meta-atoms ($\Delta\varphi_m$) is a constant at target frequency f_0 [see Fig. 1(a)] or, within a frequency interval from f_1 to f_2 [see Fig. 1(b)], the incident waves are bent to angles linked with wavelengths, and the deflection angle at the low frequency of f_1 is larger than that at the high frequency of f_2. When $\theta_i(f_i)$ equals a constant angel θ_0 within the frequency band [see Fig. 1(c)], an achromatic meta-mirror can be obtained.[17–26] In this case, φ_m is linear against frequency while having different slopes for meta-atoms at different locations, and an abnormal chromatic meta-mirror can be achieved if $\theta_i(f_i)$ changes as a function of frequency [see Fig. 1(d)].

Next, we use the effective medium theory to manipulate the dispersion distributions of a reflective meta-atom.[44–47] A typical reflective meta-atom is a sandwich structure, composed of a metallic patch resonator with size $a_1 \times b_1$ and a continuous metal sheet, separated by a 1-mm-thick F4B spacer, as shown in the inset of Fig. 2(c), which can be well described by a Lorentz model. The F4B spacer has been considered as the dielectric losses by assuming the dielectric constant as $\varepsilon_r = 2.65 + 0.01i$, and the metal is considered a perfect electric conductor since the meta-atom is working in the microwave regime. Figure 2(b) shows the effective-medium model of such a reflective metasurface. For a single resonant meta-atom, the Lorentz model can be described as

$$\mu_{2eff} = 1 - \frac{\omega_p^2}{\omega^2 - \omega_0^2 + i\omega\gamma}, \tag{2}$$

where ω_0, ω_p, and γ are the resonance, plasma, and damping frequencies.[45,47] The reflection coefficient can be calculated using the 2×2 TMM as $r = -Q_{21}/Q_{22}$, with Q being the transfer matrix.[45,47] We can tune ω_0 and ω_p to obtain different reflection phase spectra by optimizing the patch structural parameter b_1 and a_1 in a realistic meta-atom. High agreements between TMM and the finite-difference-time-domain (FDTD) simulations in Fig. 2(c) are clearly observed when $f_0 = 2\pi\omega_0 = (8.1, 10.2, 12.2)$ GHz, $f_p = (60, 60, 60)$ GHz, and
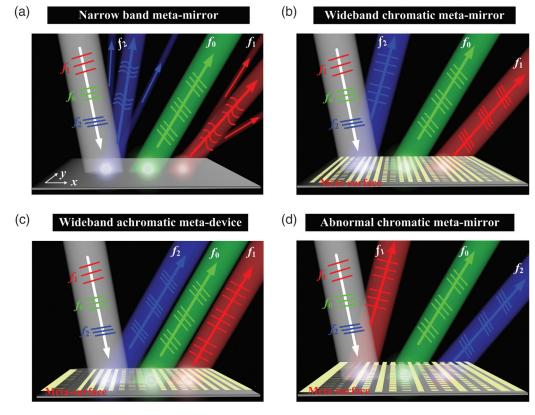
Fig. 1 Schematics and working principles of highly efficient and wideband chromatic aberration-free meta-mirrors. (a) Typical scattering patterns of narrow band meta-mirrors with high performance only at the frequency of f_0, while other scattering modes, such as the specular reflection, appear at nonworking frequencies. Typical scattering patterns of (b) wideband chromatic meta-mirror, (c) achromatic meta-mirror, and (d) abnormal chromatic meta-mirror with high performance within a wide bandwidth. The reflection angle at low frequency f_1 is larger than that at high frequency f_2 for (a) and (b) for the same phase gradients within the frequency interval from f_1 to f_2. The reflection angle for the achromatic meta-mirror is the same as shown in (c). While the reflection angle satisfies a linear function for the abnormal chromatic meta-mirror in (d), the larger frequency f_2 exhibits a larger reflection angle. The frequencies satisfy $f_2 > f_0 > f_1$.

$b_1 = (9.4, 8, 6.5)$ mm, respectively. The phase undergoes continuous -180 deg to 180 deg as the resonant frequency f_0 decreases gradually, as the reflection phase map shown in Fig. 2(d). However, the obviously resonant curves cannot satisfy the requirement of arbitrary dispersion calculated in Eq. (1), and the phase variation range is limited within -180 deg to 180 deg. Therefore, the single resonant meta-atom is unable to design chromatic aberration-free meta-devices.

We solve the issues by constructing a multiresonant model. The reflection phase variation range can be enlarged by mutual interactions among multiresonant systems,[32,48,49] and the phase spectra slope can be modulated by carefully tuning these resonances. A Lorentz model with n resonances can be expressed as

$$\mu_{2\text{eff}} = 1 - \frac{\omega_{1p}^2}{\omega^2 - \omega_1^2 + i\omega\gamma_1} - \dots - \frac{\omega_{ip}^2}{\omega^2 - \omega_i^2 + i\omega\gamma_i} - \dots$$
$$- \frac{\omega_{np}^2}{\omega^2 - \omega_n^2 + i\omega\gamma_n}. \tag{3}$$

With ω_i, ω_{ip}, and γ_i being the i'th resonance, plasma, and damping frequencies. We demonstrate this model by the dual-resonant meta-atom composed of a double-layered patch structure. Referring to Fig. 2(e), we can see that the reflection phase spectra calculated by FDTD can also coincide with those TMM results by properly tuning f_1 (ω_1) and f_2 (ω_2). To show clearly the effect of resonant frequency on φ_m, Fig. 2(f) plots the dependence of the reflection phase spectra on f_1. We can see that the phases change significantly at the low-frequency band while keeping nearly consistent in the high-frequency range, since the phase at low frequency is predominantly determined by f_1. Oppositely, the phase spectra are quite insensitive at the low-frequency bands but are sensitive in the high-frequency range, as we only vary f_2; see details in Sec. A of the Supplemental Materials. By interchanging f_1 and f_2, we can obtain a reflection phase map considering all dual resonances, which is summarized in Sec. A of the Supplemental Materials. From this map, we can successfully find some linear phase spectra at the frequency band of 8 to 12 GHz, while the phase variation range is still limited, inconvenient for the design of ultrawideband chromatic aberration-free meta-devices. Continuing to increase the number of resonances can further improve the phase variation range, while the realistic structure becomes more complex. Therefore, it is a tradeoff between the
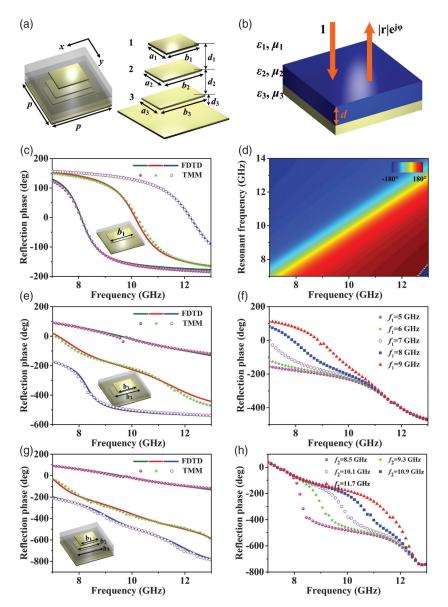
Fig. 2 Meta-atom design and EM response calculated by the TMM on the effective model and FDTD simulations on realistic structures. (a) Schematics of the proposed composite meta-atom composed of four metallic layers separated by three F4B spacers ($\varepsilon_r = 2.65 + 0.01i$, $p = 10$ mm, $d_1 = 2$ mm, $d_2 = 1$ mm, $d_3 = 0.5$ mm). Other parameters b_1, b_2, b_3 and a_1, a_2, a_3 are tuned for each meta-atom. (b) The geometry of the proposed effective model to equivalently describe the multiresonant meta-atoms. TMM computed reflection phase spectra with different resonant frequencies f_i and FDTD simulated case with different structural parameters for (c) single-resonant, (e) dual-resonant, and (g) three-resonant elements. The inset shows the corresponding schematics. The polarization is along x direction in all cases. For the single resonance at (c), $a_1 = 5$ mm, $b_1 = 6.5$, 8, and 9.4 mm for the blue, red, and green lines of the FDTD simulations, and $f_1 = 8.1$, 10.2, and 12.2 GHz for the pink, green, and blue symbols of the TMM calculations. For the double resonances at (e), $a_1 = a_2 = 4$ mm, $b_1 = 5$, 6, and 9 mm, $b_2 = 5$, 8.2, 9.5 mm for the green, red, and blue lines of the FDTD simulations, and $f_1 = 7$, 6, 5 GHz, $f_2 = 11.7$, 11.0, 8.3 GHz for the pink, green, and blue symbols of the TMM calculations. For the three resonances at (g), $a_1 = a_2 = a_3 = 5$ mm, $b_1 = 5, 5.5, 9$ mm, $b_2 = 5, 6.7, 9$ mm, $b_3 = 8, 8.7, 9.5$ mm for the green, red, and blue lines of the FDTD simulations, and $f_1 = 8.4, 7.5, 5$ GHz, $f_2 = 11.3, 10.2, 8.2$ GHz, $f_3 = 15.4, 12.9, 10.1$ GHz for the pink, green, and blue symbols of the TMM calculations. (d) Reflection spectra map as a function of operating frequency and resonant frequency with the plasma frequency fixed at $f_p = 18$ GHz. (f) Dependence of reflection phase spectra at f_1 for dual-resonant model computed by TMM with $f_2 = 11.7$ GHz, $f_{p1} = 6$ GHz, and $f_{p2} = 7$ GHz. (h) Dependence of reflection phase spectra on f_2 for three-resonant model computed by TMM with $f_1 = 7.5$ GHz, $f_3 = 12.9$ GHz, $f_{p1} = 5$ GHz, $f_{p2} = 4$ GHz, and $f_{p3} = 6$ GHz.

structure complexity and manipulation capability of φ_m. Finally, a Lorentz model with three resonances is selected, realized by a three-layered composite meta-atom. Figure 2(a) shows the schematic of a typical meta-atom composed of four metallic layers separated by three F4B dielectric spacers (total thickness of 3.5 mm). The mutual interactions among four metallic layers can induce three magnetic resonances, as seen in Sec. B of the Supplemental Materials. The resonant intension and the resonant interval can help tune the dispersion. Meanwhile, the Lorentz model can describe the realistic meta-atoms by carefully tuning the corresponding resonant frequencies f_1, f_2, and f_3. Similar to the dual resonant model, we can independently control the phase distributions at different frequency intervals (low, intermediate, or high band) by varying the corresponding resonant frequency. Figure 2(h) shows the effect of resonant frequency f_2 on the reflection phase, where only the intermediate band responds sensitively. The detailed phase modulation at the low/high-frequency bands and the reflection phase maps by scanning f_1, f_2, and f_3 are provided in Sec. C of the Supplemental Materials. Although we ignore the coupling effect in the theoretical Lorentz model, the variation trend of the phase profile is consistent with that of the realistic meta-atom. Thus, the obtained reflection maps from the theoretical model can help us retrieve the corresponding resonances to the predesigned φ_m and guide us to find the realistic meta-atoms quickly. For demonstration, Fig. 2(g) shows three representative linear phase spectra obtained by the TMM model and the corresponding realistic meta-atoms. The desirable φ_m and high reflection amplitude (near unit) make a promise toward high-efficiency and ultrawideband chromatic aberration-free meta-devices. The bandwidth can be further extended by introducing more resonators. However, it is limited by the modulation freedom of the phase dispersion and also the meta-atom size, and the ratio of the up and low frequencies is about $2 : 1$.[53] In the following two sections, we will discuss two examples to illustrate our strategy and demonstrate the flexibility of dispersion manipulation for the meta-atoms.

3 Results

3.1 Achromatic Meta-Mirror

We first design an achromatic meta-mirror with high-efficiency and ultrawideband properties using the proposed three-layered meta-atoms. To this end, the beam deflection angle at the frequency interval is set to be 30°, with Eq. (1) calculated as

$$\varphi_m(r, \lambda_i) = -\frac{2\pi}{\lambda_i}\sin\left(\frac{\pi}{6}\right)N_i p + \varphi_0 = -\frac{\pi}{\lambda_i}N_i p + \varphi_0, \qquad (4)$$

with N_i being the i'th number of meta-atoms, and the total number is set as $N = 20$. Figure 3(a) shows the calculated reflection phase distributions as a function of element number and frequency. Completely different from the reported beam deflectors,[9–12] there are no supercells in our design, and thus the phase can be tuned to vary as a linear function against the frequency with different slopes. To satisfy the unique requirement of phases, we retrieved the resonant frequencies in Eq. (3) from the reflection phase map in Fig. S3 in the Supplemental Materials. Then, we fixed the structural size of b_1, b_2, b_3 and a_1, a_2, a_3 of all meta-atoms to simultaneously satisfy these resonances, with the detailed parameters recorded

in Sec. D of the Supplemental Materials. To validate our design, we fabricated an achromatic sample containing 20×20 meta-atoms and occupying a total area of $200\ \text{mm} \times 200\ \text{mm}$. Figures 3(b)–3(d) show the photographs of the fabricated sample at different layers. The fabricated meta-atom reflection phase, phase differences compared with the theoretical case, and also the amplitude distribution are estimated in Sec. D of the Supplemental Materials. We note that the phase profiles of the fabricated meta-device match well with Eq. (4); meanwhile, the reflection amplitudes exhibit high values ($|r_{xx}| > 0.94$).

With the fabricated sample in hand, we experimentally demonstrate its achromatic and high-efficiency performances. The achromatic property is considered first by measuring the scattering patterns within the operating frequency band. Illuminating an $\hat{x}$-polarized microwave (7 to 13 GHz) normally onto our meta-device, we detected the angular distributions of scattered waves at the reflection side of the metasurface. As shown in Fig. 3(f), within our target frequency band (8 to 12 GHz), most incident EM waves are reflected to an identical angle 30°, as predesigned in Eq. (4), with the angle further confirmed by the measured and simulated radiation patterns shown in Fig. 3(g). More importantly, other undesired modes are totally suppressed, leaving only the anomalous reflection mode to survive, which implies high working efficiency of the designed achromatic meta-mirror. The FDTD simulations are performed to well reproduce almost all measured results, which are shown in Fig. 3(e). While outside the operating band, undesired modes, especially the specular reflections, increase significantly,[31,32,40] and the deflection angle shifts slightly from the theoretical case. To understand the physics of the achromatic property, we measure the electric field distributions on the xoz plane at the reflection space. As shown in Fig. 4(a), the electric field, including amplitude and phase information, is recorded by a self-designed monopole antenna ($\sim$20 mm long) as our meta-device shined by an $\hat{x}$-polarized plane wave. To see clearly the beam-bending effect, we deduce the incident field (obtained by repeating the measurement by moving away the meta-mirror[28,32] from the measured results, thus we can get only the scattered field). Figures 4(b)–4(f) show the Re$[E]$ distributions at the frequency interval of 8 to 12 GHz in the step of 1 GHz. The very clean beam bending signature and the exact deflection angles of 30° reinforce our notion of achromatism and high working efficiencies in a wide bandwidth.

Then, we quantitatively characterize the working efficiency of our achromatic meta-mirror. The efficiency is defined as the ratio between the power taken by the desired anomalously deflected mode and the incident power at different frequencies.[31,32] We experimentally obtain the power carried by the desired mode by integrating the scattered wave over an appropriate angle region at each frequency, while the incident power is calculated by integrating over the angle region of the specularly reflected mode when the metasurface is replaced by a metallic plate of the same size. Figure 3(h) shows the experimental and simulated efficiencies as a function of frequency. At the target frequency band of 8 to 12 GHz, the absolute efficiencies of our meta-device are within the range of 85% to 91% retrieved from our experimental results, and it is 85% to 94% based on the FDTD simulations, where the missing power is taken away by the dielectric loss ($\sim$2% to 4% in both simulations and measurements) and other undesirable reflection. The slight difference between the simulation and
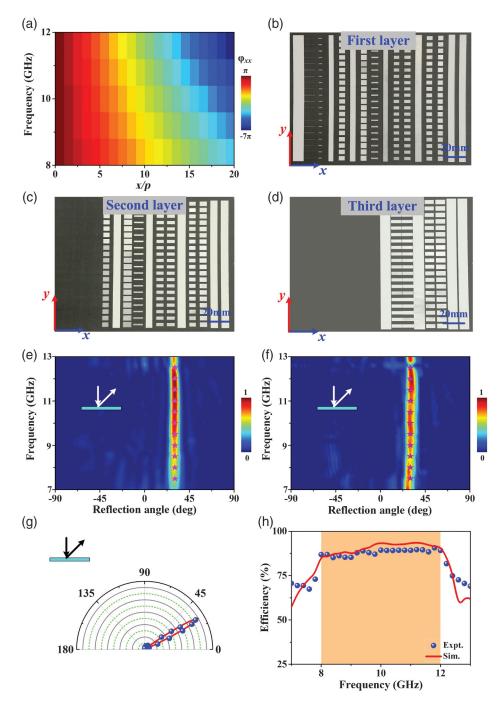
Fig. 3 Design and performance of the achromatic meta-mirror. (a) Theoretically calculated phase profiles at the target frequency band. The pictures on the (b) first layer, (c) second layer, and (d) third layer of the fabricated achromatic meta-mirror. (e) FDTD simulated and (f) measured scattered-field intensity (color map) versus frequency and detected angles at the reflection space of the meta-device shined by $\hat{x}$-polarized microwaves. (g) The measured (symbols) and simulated (solid line) scattering patterns of our metasurface illuminated by an $\hat{x}$-polarized wave at the frequency $f_0 = 10$ GHz. (h) FDTD simulated and measured absolute efficiencies of the meta-device. All of the electric field intensities are normalized against the maximum value in the spectra.

measurement is attributed to inevitable fabrication errors and imperfections of the incoming wavefronts generated by our microwave horns. Outside the band, the efficiency decreases rapidly due to the uncontrolled dispersion φ_m, which is similar to the reported cases.[9–33,54]

3.2 Abnormal Chromatic Meta-Mirror

As the second example, we design an abnormal chromatic meta-mirror by manipulating the bending angles as a linear function of frequency. To not lose generality, the deflection angles $\theta_i(f_i)$
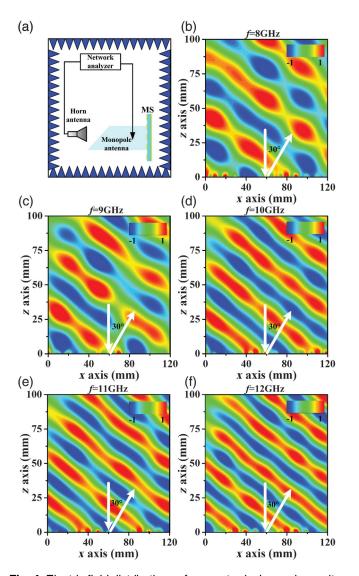
Fig. 4 Electric field distributions of our meta-device under excitation of $\hat{x}$-polarized waves. (a) Experimental setup of the near-field measurement. Measured $\mathrm{Re}[\vec{E}]$ distributions on the xoz plane at the reflection side of our metasurface at (b) 8 GHz, (c) 9 GHz, (d) 10 GHz, (e) 11 GHz, and (f) 12 GHz under excitation of normally incident $\hat{x}$-polarized waves. All of the electric field spectra are normalized against the maximum value at each frequency.

are set as $\theta_i(f_i) = 8 + 2f_i$, with the unit of f_i in GHz and θ_i in degrees. Therefore, the designed meta-device should exhibit the following phase distributions:

$$\varphi_{\mathrm{m}}(r, \lambda_i) = -\frac{2\pi}{\lambda_i}\sin(8 + 2f_i)N_i p + \varphi_0. \qquad (5)$$

To the best of our knowledge, it is the first time for controlling the deflection angle within broadband using a passive approach, because the dispersion of the passive materials is very difficult to control as desirable.[50,51] Here, we break the fixed relation of the deflection angle within the working band using the Lorentz model and extend the freedom of wavefront manipulation capability significantly for the meta-mirrors. The meta-atom number is fixed as $N = 16$. Figure 5(a) plots the theoretical reflection

phase spectrum for each meta-atom as a function of frequency. We note that the phase profiles are similar to that of the achromatic beam deflector except the phase slope, which can be used to examine the flexibility of our proposed strategy. We carefully optimize each meta-atom with its detailed structural parameters shown in Sec. E of the Supplemental Materials, together with the designed phase profiles, phase differences compared with those calculated by Eq. (5), and the amplitude distributions against frequency. The high reflection and desirable φ_{m} indicate high performance of our meta-device. For practical applications, we fabricate a meta-device sample composed of three layers, with their pictures shown in Fig. 5(b). The sample consists of 16×20 meta-atoms with a total area of 160 mm $\times$ 200 mm.

The wave-manipulation performances of this meta-mirror are also experimentally examined. We first demonstrate its ultra-broadband beam bending property. Using an identical experimental configuration with that of the achromatic meta-device, we measure the angular distributions of scattered waves under an $\hat{x}$-polarized incidence at different frequencies, with the results shown in Fig. 5(c). Within the frequency interval of 8 to 12 GHz, most incident power is reflected to an oblique angle as predesigned [solid pink star in Fig. 5(b)]. We perform FDTD simulations to calculate the scattered field distributions in Sec. F of the Supplemental Materials, which agree well with the measurements. We note clearly that the zero-order reflection mode almost disappears at the frequency band, indicating high-performance of our meta-mirror. The resultant linear beam deflection angles distinguish completely with the normal chromatic meta-mirrors, which have the same phase gradients, and their deflection angles have the fixed relation determined by the generalized Snell's law [solid white circles in Fig. 5(b)].[9–12] In fact, the normal chromatic meta-mirror with wideband and high efficiencies can also be realized by our meta-atoms [see Fig. 1(b)], with the results shown in Sec. H of the Supplemental Materials. The designed normal chromatic meta-mirror can achieve beam bending effects within 8 to 12 GHz, and the efficiencies are in the range of 90% to 95%, which is better than the reported cases.[31,32,40]

Second, we characterize the working efficiency of the designed meta-mirror. The working efficiency is calculated by integrating the anomalous reflection mode and the total power against frequencies. Figure 5(e) shows the simulated and measured results, indicating that the efficiencies are better than 85% (86%) for measurements (simulations) within the target 8 to 12 GHz, while it degrades significantly outside the band, which is due to the successfully suppressed undesired modes within the band, and the loss of the meta-device is <3.5% in the target frequency interval. We make the comparison of performances between the previous research and this work, as the results shown in Table S1 in Sec. J of the Supplemental Materials. It is obvious that the proposed chromatic aberration-free meta-mirrors achieve desirable improvements both in very high working efficiency and bandwidth enhancement. Finally, we measure the $\mathrm{Re}[\vec{E}]$ distributions by recording the electric fields at the xoz plane at different frequencies, with the results shown in Fig. 5(d). Gradually increased deflection angles against increased frequencies demonstrate the feasibility of our design for a second time, and the deflection angles are retrieved, which is totally consistent with Eq. (5). Moreover, the parallel wavefront at each frequency is highly desired, indicating the efficient phase and dispersion manipulation capability of our meta-mirror.
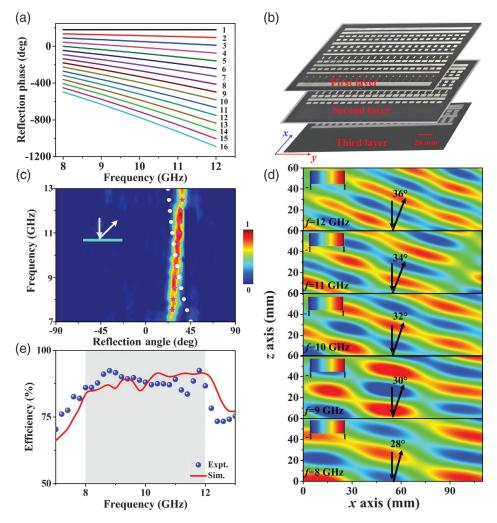
Fig. 5 Design and performance of our abnormal chromatic meta-mirror. (a) Theoretical calculated reflection phase distributions of 16 meta-atoms against frequencies. (b) Pictures of the fabricated sample of meta-mirror. (c) Measured scattered-field intensity (color map) versus frequency and detecting angles at the reflection space of the metasurface shined by $\hat{x}$-polarized microwaves. Solid pink stars denote the predesigned deflection angles computed by Eq. (5), while the solid white circles denote the deflection angles calculated by generalized Snell's law. (d) The measured $\mathrm{Re}[\vec{E}]$ distributions on the xoz plane at frequencies of 8 to 12 GHz in the step of 1 GHz. (e) Simulated and measured absolute efficiencies of the abnormal chromatic meta-mirror. All field values are normalized against the maximum value in the corresponding spectra/patterns.

4 Discussion

Our strategy to design chromatic aberration-free metadevices with high efficiencies and ultrawideband properties can work not only at the microwave but also at the high frequency band. To show this ability, we have designed a THz achromatic meta-mirror and an optical achromatic meta-mirror in reflection geometries by tuning both the material dispersion and phase properties. Similar with the microwave case, the THz achromatic meta-atom realizes the multiresonances using a composite structure consisting of four gold layers separated by three polyimide spacers. The meta-mirror can work at a broad bandwidth (0.5 to 0.8 THz) with high efficiencies (in the range of 75% to 84%), and the metal loss increases to 5% to 13%

within the target frequency interval. At the optical region, we realize our strategy to tune both reflection phase and dispersion based on multiresonant dielectric meta-atoms. Three kinds of dielectric materials with different thicknesses are optimized to reach the required phase distributions. As a result, an optical achromatic meta-mirror over a continuous wavelength region from 1150 to 1875 nm is realized, and the efficiency is in the range of 85% to 91%. The details of meta-mirror design at the high frequency region are shown in Sec. G of the Supplemental Materials. Moreover, our strategy can also help us to design other chromatic aberration-free meta-devices in the high frequency range based on the multiresonant systems, which show great superiority over those reported achromatic devices.[17,18,25,26]

5 Conclusions

We propose a strategy to design reflective chromatic aberration-free meta-mirrors with ultrawideband and high-efficiency properties by tuning both the phase dispersion and reflection amplitude. Our strategy can be easily transferred to the transmission geometry with a similar criterion except that we tune the transmission phase dispersion and transmission amplitude in this case. The reflective chromatic aberration-free meta-mirrors are analyzed using the multiresonant Lorentz model theoretically and thus achieved in realistic structures using the proposed three-layered composite meta-atom. Two kinds of microwave meta-mirrors are designed/fabricated with very high efficiencies in the frequency interval of 8 to 12 GHz (in the range of 85% to 94%). One is the achromatic meta-mirror, which can achieve the same deflection angle at different frequencies. The other one is the abnormal chromatic meta-mirror, which can deflect the incident waves as a linear function of frequency. Our results establish a solid platform to efficiently manipulate EM waves within the broad band, which can stimulate further studies related to wideband meta-devices, such as achromatic meta-lens and frequency-controlled multifunctional meta-devices, and can stimulate the realization of high-performance optical components.

6 Appendix: Experimental Setup

All microwave samples were fabricated with a standard printed-circuit-board method. We perform both near-field and far-field experiments in an anechoic chamber to avoid interferences from the environment. In our near-field measurements, a horn antenna and a monopole antenna (with the length of ~20 mm) are connected to a vector-field network analyzer (Agilent E8362C PNA) to record both the amplitude and phase information of the electric field with a pixel of 0.5 mm. The monopole antenna is digitally controlled to move in a spatial step of 0.5 mm; see Figs. 4(b)–4(f) and 5(d) for the measured $\mathrm{Re}[\vec{E}]$ distributions. In our far-field measurements, we fixed the meta-device and source antenna on a table that can rotate freely to emit the scattered signal in different directions and then used another identical antenna to receive the scattered-wave power. The receiver was placed 10 m away from the sample to guarantee that the measurement is carried out in a far-field approximation, and the results are shown in Figs. 3(f) and 5(c). More detailed information on the experimental setup can be found in Sec. I of the Supplemental Materials.

Acknowledgments

References

1. J. B. Pendry et al., "Extremely low frequency plasmons in metallic mesostructures," *Phys. Rev. Lett.* **76**(25), 4773–4776 (1996).
2. R. A. Shelby, D. R. Smith, and S. Schultz, "Experimental verification of a negative index of refraction," *Science* **292**(5514), 77–79 (2001).
3. K. Shiraishi, T. Sato, and S. Kawakami, "Experimental verification of a form-birefringent polarization splitter," *Appl. Phys. Lett.* **58**(3), 211–212 (1991).
4. H. F. Ma et al., "Independent control of differently-polarized waves using anisotropic gradient-index metamaterials," *Sci. Rep.* **4**(1), 6337 (2014).
5. D. R. Smith, J. B. Pendry, and M. C. K. Wiltshire, "Metamaterials and negative refractive index," *Science* **305**(5685), 788–792 (2004).
6. J. B. Pendry, "Negative refraction makes a perfect lens," *Phys. Rev. Lett.* **85**(18), 3966–3969 (2000).
7. D. Schurig et al., "Metamaterial electromagnetic cloak at microwave frequencies," *Science* **314**(5801), 977–980 (2006).
8. J. Li and J. B. Pendry, "Hiding under the carpet: a new strategy for cloaking," *Phys. Rev. Lett.* **101**(20), 203901 (2008).
9. N. Yu et al., "Light propagation with phase discontinuities: generalized laws of reflection and refraction," *Science* **334**(6054), 333–337 (2011).
10. X. Ni et al., "Broadband light bending with plasmonic nanoantennas," *Science* **335**(6067), 427 (2012).
11. S. Sun et al., "High-efficiency broadband anomalous reflection by gradient meta-surfaces," *Nano Lett.* **12**(12), 6223–6229 (2012).
12. A. M. H. Wong and G. V. Eleftheriades, "Perfect anomalous reflection with a bipartite Huygens' metasurface," *Phys. Rev. X* **8**(1), 011036 (2018).
13. L. Li et al., "Electromagnetic reprogrammable coding-metasurface holograms," *Nat. Commun.* **8**(1), 197 (2017).
14. X. Zhu et al., "Resonant laser printing of structural colors on high-index dielectric metasurfaces," *Sci. Adv.* **3**(5), e1602487 (2017).
15. M. Khorasaninejad et al., "Broadband and chiral binary dielectric meta-holograms," *Sci. Adv.* **2**(5), e1501258 (2016).
16. G. Zheng et al., "Metasurface holograms reaching 80% efficiency," *Nat. Nanotechnol.* **10**(4), 308–312 (2015).
17. F. Aieta, M. A. Kats, and F. Capasso, "Multiwavelength achromatic metasurfaces by dispersive phase compensation," *Science* **347**(6228), 1342–1345 (2015).
18. J. Ding et al., "Dual-wavelength terahertz metasurfaces with independent phase and amplitude control at each wavelength," *Sci. Rep.* **6**(1), 34020 (2016).
19. O. Avayu et al., "Composite functional metasurfaces for multi-spectral achromatic optics," *Nat. Commun.* **8**(1), 14992 (2017).
20. M. Khorasaninejad and F. Capasso, "Metalenses: versatile multifunctional photonic components," *Science* **358**(6367), eaam8100 (2017).
21. M. Khorasaninejad et al., "Achromatic metalens over 60 nm bandwidth in the visible and metalens with reverse chromatic dispersion," *Nano Lett.* **17**(3), 1819–1824 (2017).
22. S. L. Sun et al., "Electromagnetic metasurfaces: physics and applications," *Adv. Opt. Photonics* **11**(2), 380–479 (2019).
23. Y. Zhou et al., "Multilayer noninteracting dielectric metasurfaces for multiwavelength metaoptics," *Nano Lett.* **18**(12), 7529–7537 (2018).
24. E. Arbabi et al., "Controlling the sign of chromatic dispersion in diffractive optics with dielectric metasurfaces," *Optica* **4**(6), 625–632 (2017).
25. W. T. Chen et al., "A broadband achromatic metalens for focusing and imaging in the visible," *Nat. Nanotechnol.* **13**(3), 220–226 (2018).
26. S. Wang et al., "A broadband achromatic metalens in the visible," *Nat. Nanotechnol.* **13**(3), 227–232 (2018).
27. S. Sun et al., "Gradient-index meta-surfaces as a bridge linking propagating waves and surface waves," *Nat. Mater.* **11**(5), 426–431 (2012).
28. W. Sun et al., "High-efficiency surface plasmon meta-couplers: concept and microwave-regime realizations," *Light Sci. Appl.* **5**(1), e16003 (2016).
29. A. D. Dunkelberger et al., "Active tuning of surface phonon polariton resonances via carrier photoinjection," *Nat. Photonics* **12**(1), 50–56 (2018).
30. M. Ramezani et al., "Plasmon-exciton-polariton lasing," *Optica* **4**(1), 31–37 (2017).

31. T. Cai et al., "High-performance bifunctional metasurfaces in transmission and reflection geometries," *Adv. Opt. Mater.* **5**(2), 1600506 (2017).
32. T. Cai et al., "High-efficiency and full-space manipulation of electromagnetic wave-fronts with metasurfaces," *Phys. Rev. Appl.* **8**(3), 034033 (2017).
33. C. Pfeiffer et al., "High performance bianisotropic metasurfaces: asymmetric transmission of light," *Phys. Rev. Lett.* **113**(2), 023902 (2014).
34. X. Wan et al., "Multichannel direct transmissions of near-field information," *Light Sci. Appl.* **8**(1), 60 (2019).
35. Y. Yang et al., "Full-polarization 3D metasurface cloak with preserved amplitude and phase," *Adv. Mater.* **28**(32), 6866–6871 (2016).
36. C. Qian et al., "Experimental observation of superscattering," *Phys. Rev. Lett.* **122**(6), 063901 (2019).
37. C. Wang et al., "Superscattering of light in refractive-index near-zero environments," *Prog. Electromagn. Res.* **168**, 15–23 (2020).
38. F. Sun et al., "A camouflage device without metamaterials," *Prog. Electromagn. Res.* **165**, 107–117 (2019).
39. B. Zheng et al., "Remote concealing any arbitrary objects with multi-folded transformation optics," *Light Sci. Appl.* **5**(12), e16177 (2016).
40. W. Luo et al., "Photonic spin hall effect with nearly 100% efficiency," *Adv. Opt. Mater.* **3**(8), 1102–1108 (2015).
41. M. Jia et al., "Efficient manipulations of circularly polarized tera-hertz waves with transmissive metasurfaces," *Light Sci. Appl.* **8**(1), 16 (2019).
42. J. Zhang et al., "Plasmonic metasurfaces with 42.3% transmission efficiency in the visible," *Light Sci. Appl.* **8**(1), 53 (2019).
43. X. Ding et al., "Ultrathin pancharatnam-berry metasurface with maximal cross-polarization efficiency," *Adv. Mater.* **27**(7), 1195–1200 (2015).
44. C. Qu, et al., "Tailor the functionalities of metasurfaces based on a complete phase diagram," *Phys. Rev. Lett.* **115**(23), 235503 (2015).
45. J. Hao et al., "Manipulating electromagnetic wave polarizations by anisotropic metamaterials," *Phys. Rev. Lett.* **99**(6), 063908 (2007).
46. D. Ye et al., "Ultrawideband dispersion control of a metamaterial surface for perfectly-matched-layer-like absorption," *Phys. Rev. Lett.* **111**(18), 187402 (2013).
47. L. Zhou et al., "Electromagnetic-wave tunneling through negative-permittivity media with high magnetic fields," *Phys. Rev. Lett.* **94**(24), 243905 (2005).
48. T. Cai et al., "Ultra-thin polarization beam splitter using 2-D transmissive phase gradient metasurface," *IEEE Trans. Antennas Propag.* **63**(12), 5629–5636 (2015).
49. F. Monticone, N. M. Estakhri, and A. Alù, "Full control of nanoscale optical transmission with a composite metascreen," *Phys. Rev. Lett.* **110**(20), 203903 (2013).
50. H.-T. Chen et al., "Active terahertz metamaterial devices," *Nature* **444**(7119), 597–600 (2006).
51. H. X. Xu et al., "Tunable microwave metasurfaces for high-performance operations: dispersion compensation and dynamical switch," *Sci. Rep.* **6**(1), 38255 (2016).
52. K. W. Allen et al., "Multi-objective genetic algorithm optimization of frequency selective metasurfaces to engineer Ku-passband filter responses," *Prog. Electromagn. Res.* **167**, 19–30 (2020).
53. T. Cai et al., "High-performance transmissive meta-surface for C-/X-band lens antenna application," *IEEE Trans. Antennas Propag.* **65**(7), 3598–3606 (2017).
54. L. Zhang et al., "Ultra-thin high-efficiency mid-infrared transmissive Huygens meta-optics," *Nat. Commun.* **9**(1), 1481 (2018).

Tong Cai received his BS and PhD degrees in electrical engineering from the Air Force Engineering University, Xi'an, China, in 2012 and 2017, respectively. He was with the Air Force Engineering University, where he became a lecturer in 2017 and an associate professor in 2020. He has been a postdoctoral researcher with Zhejiang University since 2019. His research interests include metamaterials, metasurfaces, and their applications to antennas and multifunctional devices.

Bin Zheng received his BS degree from Ningbo University, Ningbo, China, in 2010, and his PhD from Zhejiang University, Hangzhou, China, in 2015. He has been a postdoctoral researcher with Zhejiang University since 2015. He was with Zhejiang University, where he became a lecturer in 2017 and an associate professor in 2019. His research interests include transformation optics, metamaterials, metasurfaces, and invisibility cloaks.

Hongsheng Chen received his BS and PhD degrees in electrical engineering from Zhejiang University, China, in 2000 and 2005, respectively. He was with Zhejiang University, where he became an assistant professor in 2005, an associate professor in 2007, and a full professor in 2011. In 2014, he was honored with the Distinguished Chang Jiang Scholar Professorship by the Ministry of Education, China. His current research interests are in the areas of metamaterials, antennas, invisibility cloaking, transformation optics, and theoretical and numerical methods of electromagnetics.

Biographies of the other authors are not available.